Microstructure and enhanced mechanical properties of an Mg–10Gd–2Y–0.5Zr alloy processed by cyclic extrusion and compression

Tao Peng[a], Qudong Wang[a,b,*], Jinbao Lin[a,c], Manping Liu[a,d], Hans J. Roven[d]

[a] National Engineering Research Center of Light Alloy Net Forming, Shanghai Jiao Tong University, Shanghai 200240, China

[b] State Key Lab of Metal Matrix Composites, Shanghai Jiao Tong University, Shanghai 200240, China

[c] School of Applied Science, Taiyuan University of Science and Technology, Taiyuan 030024, China

[d] Department of Materials Science and Engineering, Norwegian University of Science and Technology, Trondheim 7491, Norway

Abstract The evolution of microstructure and texture of an extruded GW102K Mg alloy processed by cyclic extrusion and compression (CEC) at 450 °C were investigated. Tensile tests were performed at room temperature and strain rate 5×10^{-3} s^{-1}. The results show that the microstructure was effectively refined, and the initial fiber texture became disintegrated and developed a new texture after 14 CEC passes. It was found that the strength and ductility were simultaneously increased as compared with the as-extruded alloy. In particular, the elongation and yield strength were related in a line relationship having a positive slope. As the texture changed and texture intensity decreased, substantial grain refinement was observed. The hard second-phase particles were considered to be responsible for the uncommon properties of CEC processed GW102K alloy.

Keywords: Magnesium alloys; Mg–Gd–Y–Zr alloy; Mechanical properties; Cyclic extrusion compression (CEC); Microstructure; Dynamic precipitation

1. Introduction

Magnesium alloys are becoming increasingly attractive for potential use in a wide range of structural applications, including the automotive industry, because of their low density, good machinability, excellent damping capacity and favorable recycling capability [1, 2]. Nevertheless, to be used for structural components, the material should exhibit an attractive specific strength as well as sufficient ductility since components may fail by fracture due to shear or tensile forces [3]. Thus, to enable their widespread application, the relatively low strength and ductility of Mg alloys is a major difficulty that must be overcome.

Recent researches have found that the magnesium alloys processed by equal channel angular extrusion (ECAE) i.e., one kind of severe plastic deformation (SPD), show increased elongation in combination with a reduced yield strength [3-7]. This phenomenon derived from the changed texture and the refined grains after the ECAE processing. These studies mainly focused on the AZ type Mg alloys [3-5]. Conventional methods of SPD processing include ECAE, high-pressure torsion (HPT) and cyclic extrusion and compression (CEC) [8-12]. As a kind of continuous SPD processing, CEC seems to be more adaptable for industrial applications. Moreover, it is very suitable for refining grains of hard-to-deform metals such as magnesium alloys since it imposes three-dimensional compression stresses during processing [8,13]. In the past, CEC was successfully used to produce a variety of metallic materials with ultra-fine grain structures in alloys AZ31and ZK60 [8,10,13-15]. However, it is difficult to produce simultaneous increase in strength and ductility compared with the as-extruded alloy. In the present study, the Mg–10Gd–2Y–0.5Zr alloy shows a combination of high strength and excellent ductility after CEC processing. The possible improvement mechanisms are interpreted and discussed.

2. Experimental procedure

* Corresponding author. Tel.: +86-21-54742715(O); Fax: +86-21-34202794.

E-mail address: wangqudong@sjtu.edu.cn

The material used in this study is a GW102K (Mg–9.95wt%Gd–2.3wt%Y–0.46wt%Zr) magnesium alloy. For comparison, a commercial ZK60 (Mg–5.5wt%Zn–0.5wt%Zr) magnesium alloy and pure Mg were also investigated. The materials were received in the form of an extruded bar with a diameter of 29.5 mm and then cut into pieces of length 42 mm before CEC processing. The CEC die used in this investigation and its operation procedure was described elsewhere [15-17]. The CEC processing was carried out by pushing a specimen from one cylindrical chamber with a diameter D, into the second chamber with the same dimensions, through a die having a smaller diameter d. In the present study, D and d are 30 mm and 20 mm, respectively. The number of extrusion passes was defined as the number of specimen passes through the die. At the final pass, one ram was removed so that the other ram could extrude the specimen to a rod 20 mm in diameter.

After processing, the different directional microstructures of the sample were analyzed using optical microscopy (OM). Furthermore, the longitudinal sections of the samples were prepared for electron backscattered diffraction (EBSD) analyses. All other measurements were also taken along the longitudinal section of the processed materials. Samples for the EBSD study were prepared by mechanical grinding, mechanical polishing and final electropolishing with an AC2 solution, using a voltage of 15 V for 10～20 s under a controlled temperature of −30 °C. Finally, the samples were cleaned with methanol. The EBSD data collection was done in a Zeiss 55VP FEG-SEM equipped with a Nordif EBSD detector and the TSL OIM EBSD software. EBSD was performed at 20 kV, 20 mm working distance, a tilt angle of 70° and a scan step of 0.1 μm.

The flat tensile specimens with a gauge section of 10 mm × 3 mm × 1.5 mm were cut from the samples with an electric-spark wire-cutting machine. Tensile tests were carried out at room temperature and strain rate of 5×10^{-3} s^{-1}. The obtained fracture surfaces were then characterized using the SEM. Finally, the precipitated second-phase particles were analyzed using a Philips-CM20 transmission electron microscopy (TEM) operated at 200 kV.

3. Experimental results

3.1. Microstructures

Fig.1 shows the different directional microstructures of the GW102K alloy before CEC processing and after various CEC passes. The grain-size distribution was determined to be 5 ~ 25 μm, 1 ~ 10 μm, 0.5 ~ 4.5 μm and < 1 μm, respectively. With the increasing number of CEC passes, the grains became more homogenous and small. It can be seen that the microstructure of the as-received material tended to be rather heterogeneous (**Fig.1a**). After 2-passes CEC, the microstructure consisted of fine grains 1～3 μm in size and coarse grains of 8 ~ 10 μm. This kind of microstructure could be produced by dynamic - and secondary recrystallization occurring during elevated temperature plastic deformation. Secondary recrystallization could make the recrystallized fine grains to grow coarse. After 4 and 8 passes , the grains were clearly refined and became fairly homogeneous due to the believed dynamic recrystallization occuring during the deformation process.

3.2. Texture analysis

The established $\{0002\}$ and $\{10\bar{1}0\}$ pole figures are shown in **Fig.2**. Before CEC (**Fig.2a**), it was evident that {0002} basal planes and $\left\langle 10\bar{1}0 \right\rangle$ directions in most grains were distributed parallel to the extrusion direction (ED). That is, it exhibited an ED // $\left\langle 10\bar{1}0 \right\rangle$ fiber texture, which was the same as in the as-extruded ZK60 material before CEC [16]. The similar texture (i.e. basal planes lying parallel to the extrusion direction) has also been observed in other

extruded magnesium alloys [4,5,18,19]. After 4-passes CEC, the initial fiber texture became disintegrated and changed into a new $\left\{10\bar{1}3\right\}\left\langle 30\bar{3}2\right\rangle+\left\{10\bar{1}1\right\}\left\langle 1\bar{5}43\right\rangle$ type texture [13,15,16]. This dominant texture did not vary, and almost remained at the same intensity when CEC passes was increased to 8-passes from 4-passes at 450 °C. Lin et al. [16] showed the maximum intensity of both $\left\{0002\right\}$ and $\left\{10\bar{1}0\right\}$ pole figures of ZK60 magnesium alloy declined with the increasing of CEC passes. For the GW102K alloy, the maximum texture intensity of 4 and 8-passes was less than 2,5. Although the alloy was changed into one new texture, the grain orientations became very random when CEC was increased to 4 passes.

It is interesting to find that the maximum texture intensities of both $\left\{0002\right\}$ and $\left\{10\bar{1}0\right\}$ pole figures of the GW102K alloy were much lower compared with the ZK60 alloy after CEC processing [16]. In order to find the reason, both $\left\{0002\right\}$ and $\left\{10\bar{1}0\right\}$ pole figures of pure Mg and ZK60 subjected to 4-passes CEC at 350°C were also investigated in this work. As shown in **Fig.3**, the maximum intensities of both $\left\{0002\right\}$ and $\left\{10\bar{1}0\right\}$ pole figures of pure Mg were the highest, and those of GW102K were the lowest. This means that the precipitated second-phases particles caused the different texture intensities of CEC processed Mg alloys. For the ZK60 and GW102K magnesium alloys, the precipitated second-phase particles were $MgZn_2$ and $Mg_{24}(Gd,Y)_5$, respectively [16,17]. The different second-phase particles caused a different texture distribution intensity. The change in intensity occurred in spite of the fact that the texture orientation was almost the same. **Fig.4** shows the $\left\{0002\right\}$ pole plot calculated from the $\left\{0002\right\}$ pole figures of ZK60, GW102K and pure magnesium after 4-passes CEC processing at 350°C. These results also proved that the pole intensity decreased, and the maximum angle deviated from the pole equator with the precipitation of second-phase particles. During CEC processing, the second-phase particles prevented the grains to rotate, and this ability was also related to their characters. Hard, numerous second-phase particles had a strong ability to prevent the grains from rotating during the CEC processing.

3.3. Mechanical properties

The obtained values of average yield strength (YS), ultimate tensile strength (UTS) and elongation-to-failure (δ) are summarized in **Table 1**. The CEC processing does strongly alter the yield strength and the ductility. Furthermore, the tensile strength was increased to some extent. After 2-passes CEC, both the yield strength and tensile strength decreased slightly, and the elongation was somewhat enhanced. This could be ascribed to texture softening although the grains were refined to some extent. After 4 and 8 CEC passes , the elongation dramatically increased from ~ 6% of the as-received material to ~ 14% and ~ 22%, respectively, accompanied by a slight increase in the yield strength and ultimate tensile strength. When the number of passes was extended from 8 to 14, a higher yield and tensile strength were obtained though the ductility decreased. This phenomenon was probably due to grain refinement and the precipitated $Mg_{24}(Gd,Y)_5$ second-phase particles during CEC processing.

Typical SEM images of the fracture surfaces of the GW102K alloy prior to and following CEC processing are shown in **Fig. 5**. Before CEC, the fracture surface contained typical cleavage facets and cleavage steps (**Fig.5a,b**), which could be related to mechanical twinning [20]. Compared with the as-received material, the 8-passes sample exhibited obviously uniform deformation characteristics. As shown in **Fig.5c** and **Fig.5d**, there were many dimples typical of a ductile fracture after 8-passes CEC. Fracture in magnesium and magnesium alloys generally originates at deformation twins. However, after CEC processing, the formation of deformation twins was probably prevented due to texture change and grain refinement. The latter could increase activation of non-basal slip systems [21,22] and/or onset of grain boundary sliding [23].

In the dimples, second-phase particles were observed **(Fig.5c,d)**. The $Mg_{24}(Gd,Y)_5$ particles can be regarded as reinforcements in the CEC specimens, i.e. by strengthening from dislocation-particle interactions, load transfer to a lower E-modulus matrix and dislocation generation [17]. **Fig.6** shows the TEM micrograph of the alloys ZK60 and GW102K after CEC processing. Dynamically precipitated particles were observed within the grains or at the grain boundaries. The precipitated second-phase $MgZn_2$ had a small size and was uniformly distributed within the grains. On the other hand, the $Mg_{24}(Gd,Y)_5$ particles were quite large in size and distributed at the grain boundaries, which could also inhabit grain boundary sliding or lock grain boundaries. The locked grain boundaries were probably difficult to rotate during the CEC processing. Thus, the GW102K alloy could show a relatively low texture intensity after the same number of CEC passes as compared to ZK60.

4. Discussion

The changes in microstructure and mechanical properties of the GW102K alloy during CEC were clarified in the present study. The results show that after CEC processing the microstructures were clearly refined, the fiber texture became disintegrated and the $Mg_{24}(Gd,Y)_5$ phase precipitated during deformation. The CEC processing did strongly increase the yield strength and the ductility. Furthermore, the tensile strength was increased to some extent. The relationships between yield strength and elongation-to-failure prior to and following ECAE and CEC for magnesium alloys are shown in **Fig.7** [3-8]. It can be found , except for the GW102K magnesium alloy, that the common tendency is an increase in ductility in combination with a reduction in yield strength. For GW102K, the elongation and strength were related in a linear relationship having a positive slope. When comparing the results from alloy AZ31 subjected to ECAE versus CEC, CEC makes the reduction rate of strength with accompanying increase in elongation somewhat lower. However, this difference between CEC and ECAE is not very obvious, which means that, for the same AZ31 alloy, the different SPD methods can not change the negative line relationship between the yield strength and ductility.

An important result obtained in the present study is that the 14-passes CEC GW102K alloy exhibited high yield strength (270 MPa), good elongation (15%), and a linear relationship having a positive slope between the yield strength and elongation. For the ZK60 magnesium, after CEC processing, the yield strength is decreased while the elongation is notably increased. In order to explore possible reasons for this behavior, the texture change, grain size and the second-phase precipitation were considered. As shown in **Fig.4**, the pole intensity decreases with the increasing of the second-phase precipitation and the maximum angle deviated from the pole equator plane. It is therefore suggested that hard, numerous second-phase particles might have a strong ability to prevent the grains from rotating during CEC. Although the initial fiber texture became disintegrated and changed into a new $\{10\bar{1}3\}\langle 30\bar{3}2\rangle + \{10\bar{1}1\}\langle 1\bar{5}43\rangle$ type texture[13,16], the texture intensity is different after CEC. The texture intensity of the GW102K is much lower than that of ZK60 after 8-passes CEC. The lower texture intensity change, even after 14-passes CEC processing, does probably not cause the observed decrease in yield strength.

On the other hand, after 14-passes CEC of the GW102 alloy, the grains are significantly refined and the $Mg_{24}(Gd,Y)_5$ phase is precipitated. The grain refinement is favorable to an increase in yield strength according to the Hall-Petch formula. Besides, as shown in **Fig. 6**, ZK60 and GW102K can exhibit second-phase precipitation during CEC processing. In the ZK60, $MgZn_2$ precipitates have a small size and are uniformly distributed but do probably not contribute significantly to strength by particle – dislocation interactions.. However, in the GW102K, the harder $Mg_{24}(Gd,Y)_5$ phase is probably contributing more extensively to the observed strength increase. Thus, the second-phase $Mg_{24}(Gd,Y)_5$ in the CEC GW102 alloy has a positive effect on the yield strength increase due to both softening of the texture intensity and precipitate strengthening by the Orowan mechanism.

For the ductility, Koike et al. [21] have reported that the non-basal slip systems were activated as well as basal slip systems in fine grain Mg alloys due to the grain-boundary compatibility effect. These authors also concluded that, in the fine-grained AZ31B alloy, the dislocation cross-slip to non-basal planes occurred at a yield anisotropy value of only 1.1 instead of an expected value of ~100 obtained from single-crystal experiments with magnesium [21]. This

suggests that some non-basal slip systems may operate after 4-passes CEC. Furthermore, slip-induced grain-boundary sliding might be operating as a complementary deformation mechanism to give a rise to the c-axis component of strain in fine grained samples after CEC processing [22]. Thus, it can be concluded that the main contributor to the higher elongation in the present case for GW102K is due to grain refinement. Hence, grain-boundary sliding and the reduced texture intensity of CEC processed material (more random texture), may also contribute to the observed higher ductility reaching 22% after 8 passes. However, by increasing the number of CEC passes beyond 8 passes, more coarse precipitation reduced the ductility to 15% after 14 passes.

5. Conclusions

(1) The CEC processing does strongly increase the yield strength and the ductility of the GW102K alloy. Furthermore, the tensile strength is increased to some extent. For GW102K, the elongation and strength are related in a linear relationship having a positive slope, which is different from the common tendency of other Mg alloys processed by severe plastic deformation.

(2) A homogeneous structure of refined grains with a size of <1 μm is obtained after 14-passes CEC of alloy GW102K. After CEC processing, the initial fiber texture becomes disintegrated and develops a new texture. Besides, the pole intensity decreases with a more pronounced dynamic precipitation of second-phase particles. Hard, numerous second-phase particles have a strong ability to prevent the grains from rotating.

(3) The low texture intensity, the precipitated second-phase particles and grain refinement are considered to be responsible for a high yield strength even after 14-passes CEC of the GW102K alloy.

Acknowledgements This work was supported by the National Natural Science Foundation of China (No. 50674067) and the Science and Technology Commission of Shanghai Municipality (N0. 09JC1408200).

References

[1] Buha J (2008) J Mater Sci. 43: 1220.
[2] Huang X, Suzuki K, Watazu A, Shigematsu I, Saito N (2008) J Alloys Compd 457: 408.
[3] Mukai T, Yamanoi M, Watanabe H, Higashi K (2001) Scripta Mater 45: 89.
[4] Somekawa H, Mukai T (2006) Scripta Mater 54: 633.
[5] Kim WJ, Hong SI, Kim YS, Min SH, Jeong HT, Lee JD (2003) Acta Mater 51: 3293.
[6] Mehrotra P, Lillo TM, Agnew SR (2006) Scripta Mater 55: 855.
[7] del Valle JA, Carreño F, Ruano OA (2006) Acta Mater 54: 4247.
[8] Chen YJ, Wang QD, Roven HJ, Liu MP, Karlsen M, Yu YD, Hjelen J (2008) Scripta Mater 58: 311.
[9] Richert J, Richert M (1986) Aluminium 62 (8): 604.
[10] Chen YJ, Wang QD, Roven HJ, Karlsen M, Yu YD, Liu MP, Hjelen J (2008) J Alloys Compd 462: 192.
[11] Yeh JW, Yuan SY, Peng CH (1998) Mater Sci Eng A 252: 212.
[12] Richert M, Stüwe HP, Zehetbauer MJ, Richert J, Pippan R, Motz CH, Schafler E (2003) Mater. Sci. Eng. A 355: 180.
[13] Wang QD, Lin JB, Peng LM, Chen YJ (2008) Acta Metall Sin 44: 55.
[14] Lin JB, Wang QD, Peng LM, Roven HJ (2008) J Mater Sci 43: 6920.
[15] Lin JB, Wang QD, Peng LM, Peng T (2008) Mater Trans 49: 1021.
[16] Lin JB, Wang QD, Peng LM, Roven HJ (2009) J Alloys Compd 476: 441.
[17] Peng T, Wang QD, Lin JB (2009) Mater Sci Eng A516: 23.
[18] Somekawa H, Mukai T (2005) Scripta Mater 53: 541.
[19] Watanabe H, Takara A, Somekawa H, Mukai T, Higashi K (2005) Scripta Mater 52: 449.
[20] Cheng YQ, Chen ZH, Xia WJ (2007) J Mater Sci 42: 3552.

[21] Koike J, Kobayashi T, Mukai T, Watanabe H, Suzuki M, Maruyama K, Higashi K (2003) Acta Mater 51: 2055.
[22] Koike J (2004) Mater Sci Forum 449-452: 665.

Table 1 Room temperature mechanical properties of Mg–10Gd–2Y–0.5Zr alloy processed by CEC with various extrusion passes at 450℃.

Sample	YS (MPa)	UTS (MPa)	Elongation(%)
As-extruded	225	305	6
2-passes CEC	221	275	9
4-passes CEC	232	292	14
8-passes CEC	247	310	22
14-passes CEC	270	330	15

Figure captions

Fig.1 Longitudinal and transverse microstructures of the GW102K alloy (a) before CEC and after CEC: (b) 4-passes, (c) 8-passes, (d) 14-passes at 450 °C.

Fig.2 $\{0002\}$ and $\{10\bar{1}0\}$ pole figures of alloy GW102K (a) before CEC and after CEC: (b) 4-passes and (c) 8-passes at 450 °C.

Fig.3 $\{0002\}$ and $\{10\bar{1}0\}$ pole figures of pure Mg, ZK60 after 4-passes CEC deformation at 350 °C.

Fig.4 $\{0002\}$ pole plot calculated from $\{0002\}$ pole figures of ZK60, GW102K and pure magnesium after 4-passes CEC processing at 350 °C.

Fig.5 SEM morphology of fracture surfaces of the GW102K alloy before and after CEC processing: (a) and (b) as-extruded, (c) and (d) 450 °C /8-passes.

Fig.6 TEM micrographs of (a) ZK60 alloy, CEC 350 °C /4-passes and 2% elongation and (b) GW102K alloy, CEC 450 °C /8P and 2% elongation.

Fig.7 Relationship between yield strength and elongation-to-failure for magnesium alloys prior to and following SPD processing.

(a) (b)

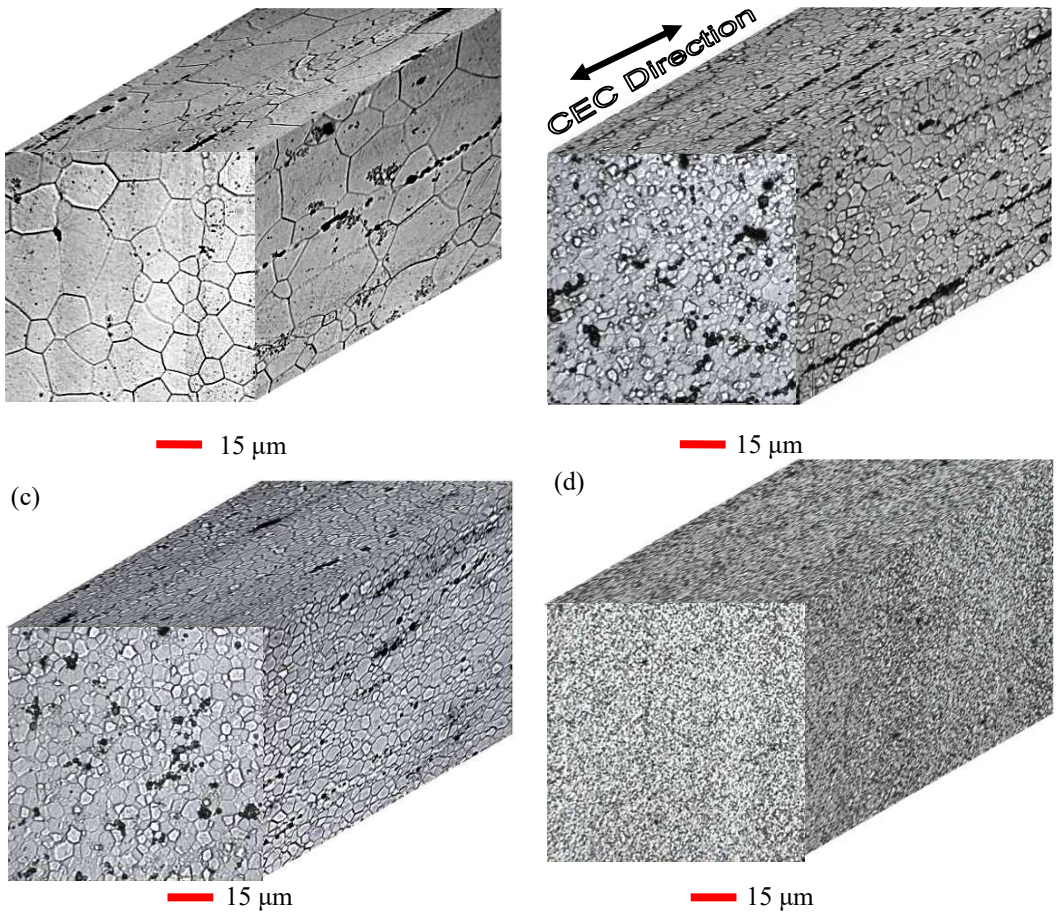

Fig.1 Longitudinal and transverse microstructures of GW102K alloy (a)before CEC and after CEC: (b) 4-passes, (c) 8-passes, (d) 14-passes at 450℃.

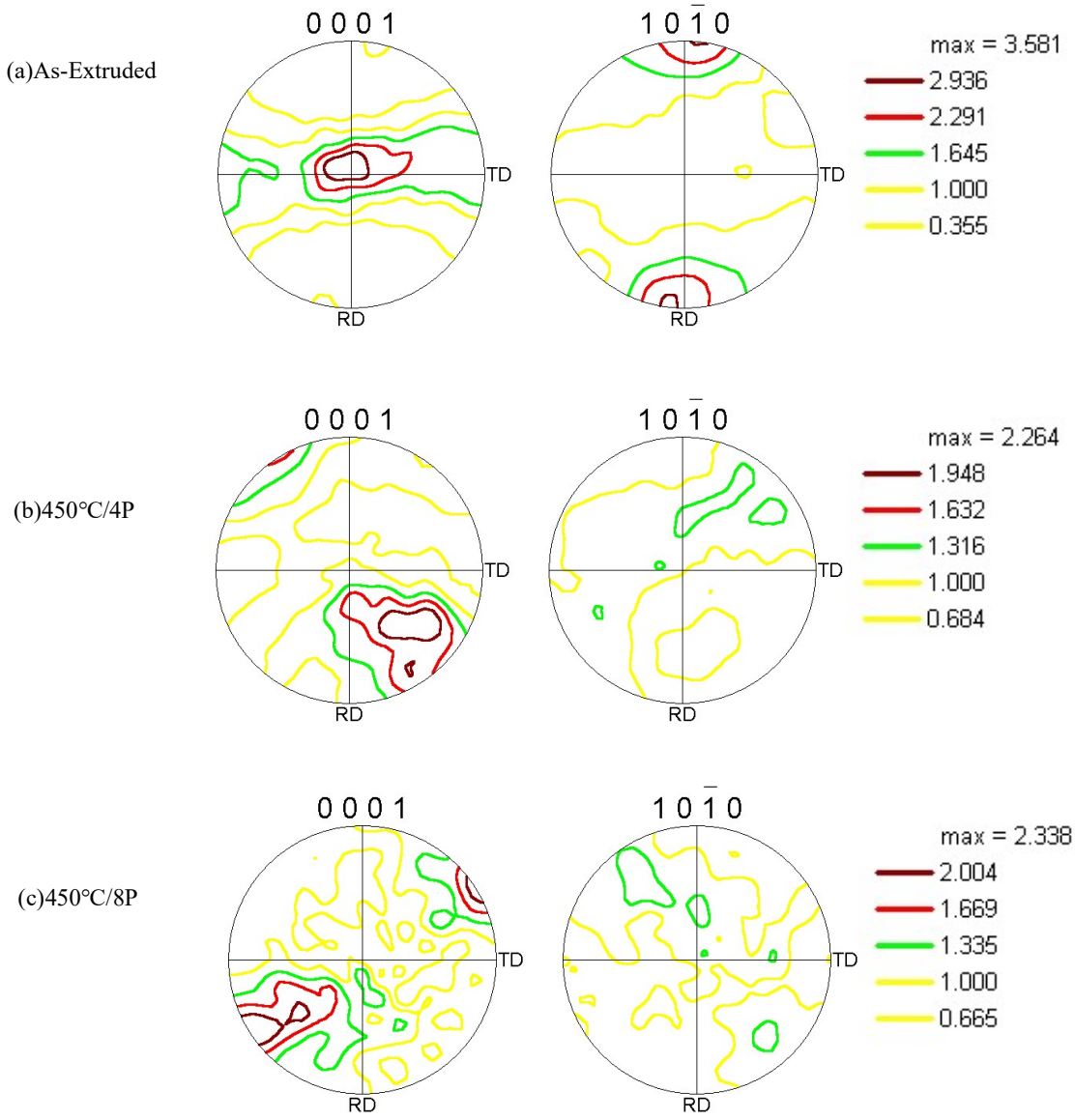

Fig.2 $\{0002\}$ and $\{10\bar{1}0\}$ pole figures of GW102K alloy (a)before CEC and after CEC: (b) 4-passes and (c) 8-passes at 450℃.

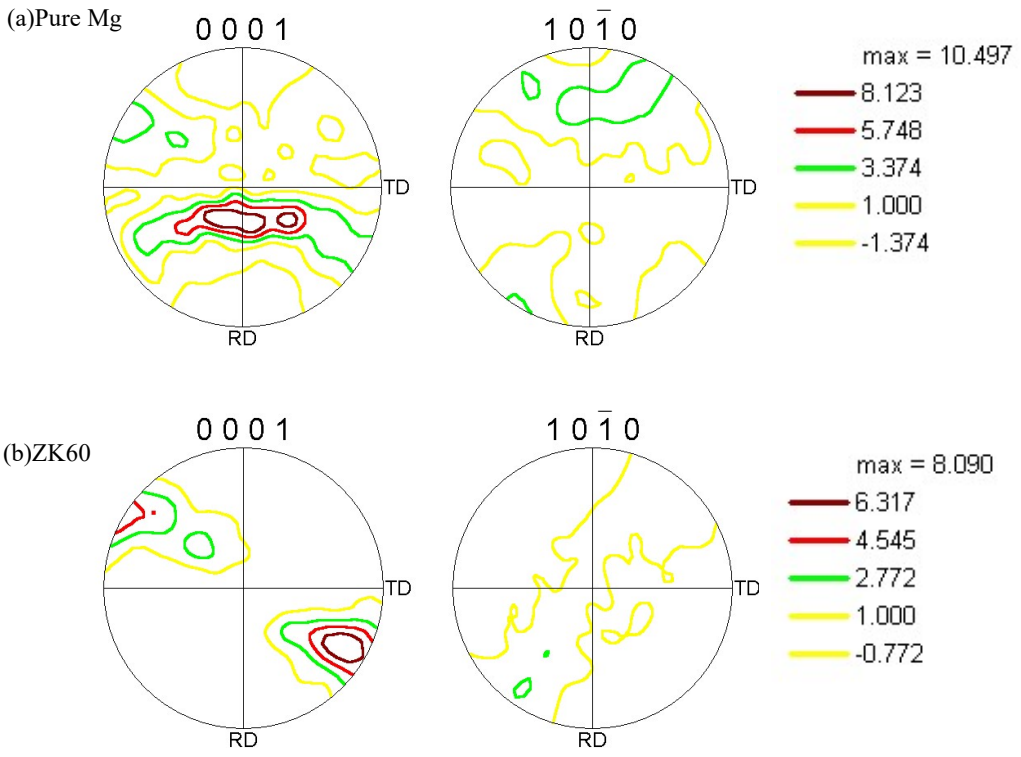

Fig.3 $\{0002\}$ and $\{10\bar{1}0\}$ pole figures of pure Mg, ZK60 after 4-passes CEC deformation at 350℃.

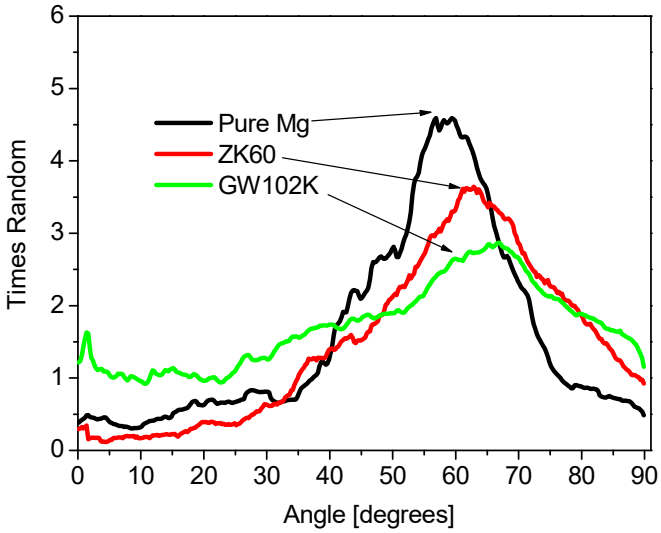

Fig.4 The $\{0002\}$ pole plot calculated from $\{0002\}$ pole figure of ZK60, GW102K and pure magnesium after 4-passes CEC processing at 350℃.

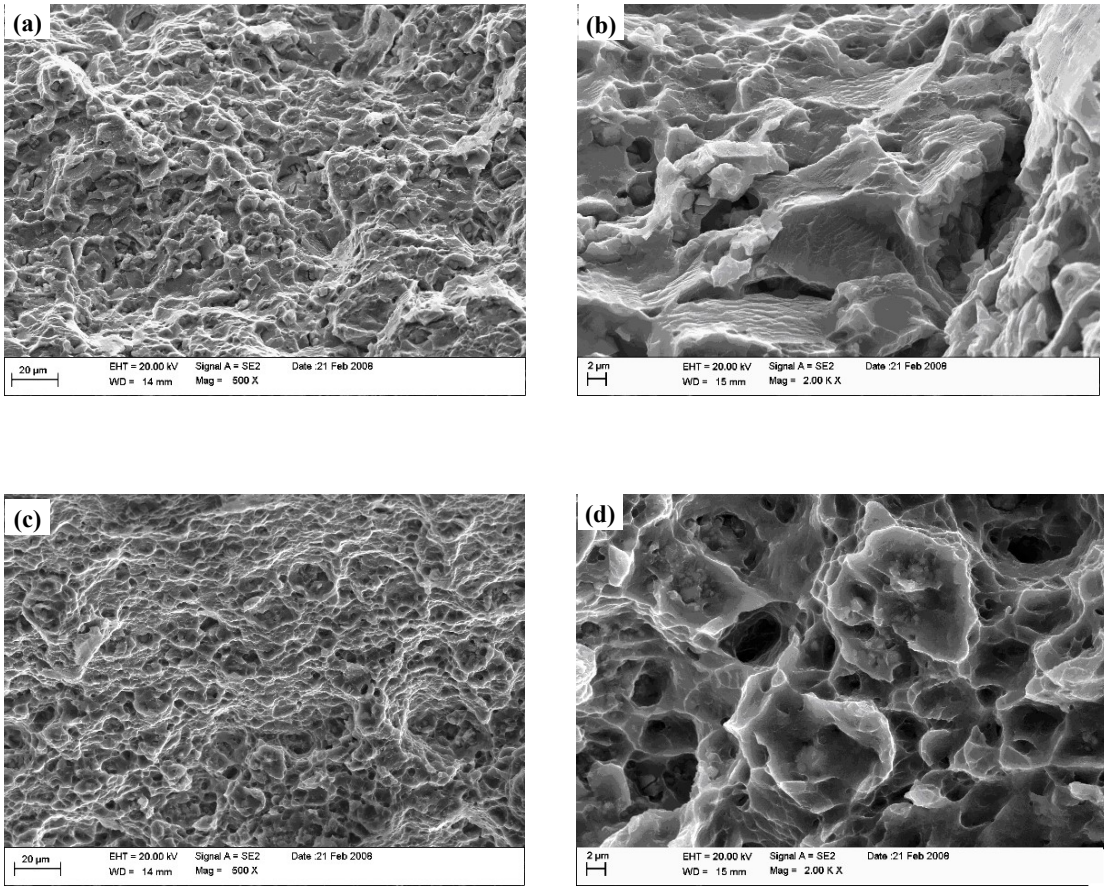

Fig.5 SEM morphology of fracture surfaces of the GW102K alloy before and after CEC processing: (a) and (b) as-extruded, (c) and (d) 450℃/8P.

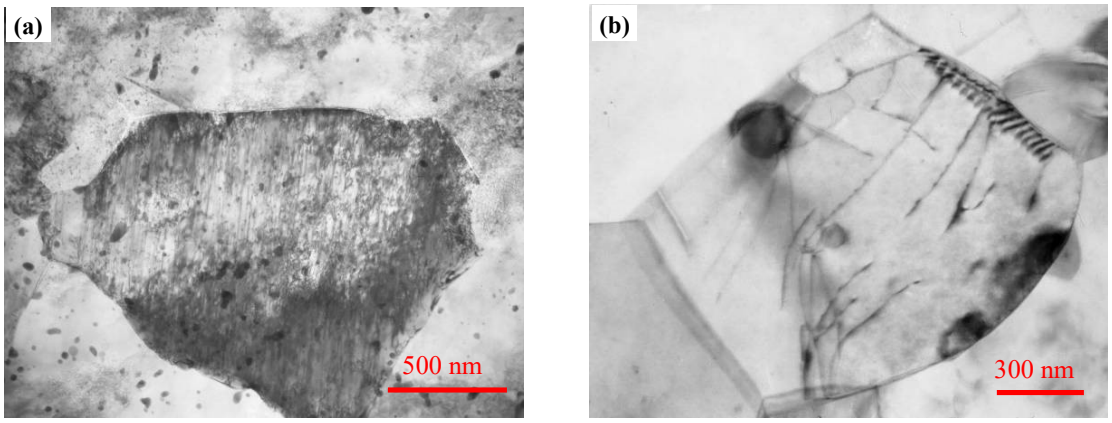

Fig.6 TEM micrographs of (a) ZK60 alloy, CEC 350℃/4P and 2% elongation and (b) GW102K alloy, CEC 450℃/8P and 2% elongation.

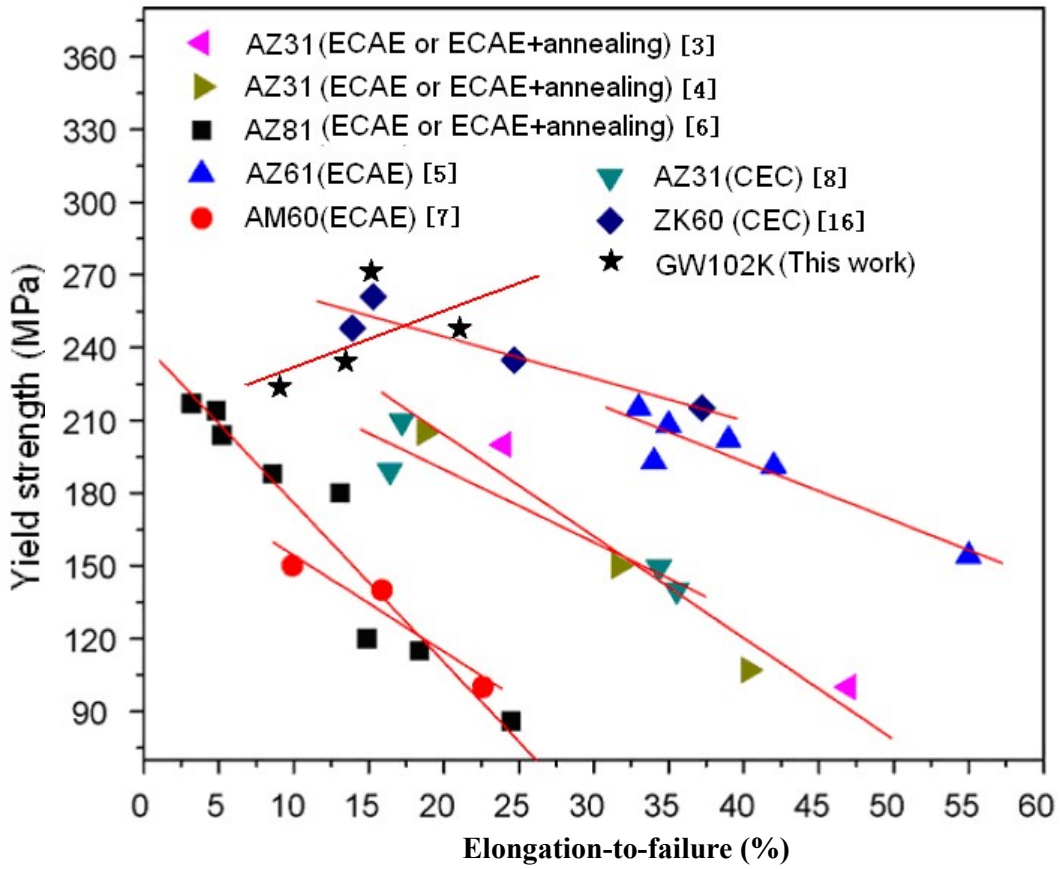

Fig.7 The relationship between yield strength and elongation-to-failure for magnesium alloys prior to and following SPD processing.